A root functional-structural model allows to assess effects of water deficit on water and solute transport parameters

Fabrice Bauget, Virginia Protto, Christophe Pradal, Yann Boursiac, Christophe Maurel

▶ **To cite this version:**

Fabrice Bauget, Virginia Protto, Christophe Pradal, Yann Boursiac, Christophe Maurel. A root functional-structural model allows to assess effects of water deficit on water and solute transport parameters. Journal of Experimental Botany, 2023, 74 (5), pp.1594-1608. 10.1093/jxb/erac471 . hal-03915413

HAL Id: hal-03915413
https://inria.hal.science/hal-03915413

Submitted on 2 Jan 2023

HAL is a multi-disciplinary open access archive for the deposit and dissemination of scientific research documents, whether they are published or not. The documents may come from teaching and research institutions in France or abroad, or from public or private research centers.

L'archive ouverte pluridisciplinaire **HAL**, est destinée au dépôt et à la diffusion de documents scientifiques de niveau recherche, publiés ou non, émanant des établissements d'enseignement et de recherche français ou étrangers, des laboratoires publics ou privés.

A root functional-structural model allows to assess effects of water deficit on water and solute transport parameters

Fabrice Bauget[1], Virginia Protto[1], Christophe Pradal[2], Yann Boursiac[1], Christophe Maurel[1*]

[1]*Institute for Plant Sciences of Montpellier (IPSiM), Univ Montpellier, CNRS, INRAE, Institut Agro, Montpellier, France.*

[2]*CIRAD, UMR AGAP Institute, Montpellier, France.*

Highlight

A model integrating water and solute transport within realistic root system architectures allows to assess the effects of water deficit on elementary root transport parameters

Accepted Manuscript

Downloaded from https://academic.oup.com/jxb/advance-article/doi/10.1093/jxb/erac471/6896019 by guest on 02 January 2023

© The Author(s) 2022. Published by Oxford University Press on behalf of the Society for Experimental Biology.
This is an Open Access article distributed under the terms of the Creative Commons Attribution License (https://creativecommons.org/licenses/by/4.0/), which permits unrestricted reuse, distribution, and reproduction in any medium, provided the original work is properly cited.

Abstract

Root water uptake is driven by a combination of hydrostatic and osmotic forces. Water transport was characterized in primary roots of maize seedlings grown hydroponically under standard and water deficit (WD) conditions, as induced by addition of 150 $g.L^{-1}$ polyethylene glycol-8000 (water potential= -0.336MPa). Flow measurements were performed by the pressure chamber technique in intact roots or on progressively cut root system architectures (RSA). To account for the concomitant transport of water and solutes in roots under WD, we developed within realistic RSAs a Hydraulic Tree Model integrating both solute pumping and leak. This model explains the high spontaneous sap exudation of roots grown in standard conditions, the non-linearity of pressure-to flow relationships, and negative fluxes observed under WD conditions at low external hydrostatic pressure. The model also reveals the heterogeneity of driving forces and elementary radial flows throughout RSA, and how this heterogeneity depends on both plant treatment and water transport mode. The full set of flow measurement data obtained in individual roots grown under standard or WD conditions was used in an inverse modeling approach to determine their respective radial and axial hydraulic conductivities. This approach allows to resolve dramatic effects of WD on these two components.

Keywords: conductance, model, root hydraulics, root system architecture, solute transport, xylem, water deficit, water transport.

Accepted Manuscript

Downloaded from https://academic.oup.com/jxb/advance-article/doi/10.1093/jxb/erac471/6896019 by guest on 02 January 2023

Introduction

The uptake of soil water by roots is crucial for the growth and survival of most of terrestrial plants. Root water uptake allows the plant to maintain its water status, under favorable or adverse environmental conditions such as drought, by continuously balancing transpirational water losses and supplying water required for expansion growth (Steudle, 2000a). Root water uptake sequentially involves a radial transport of water from the soil to the root stele and its axial transport along the root vasculature. Radial transport is mediated through cell wall (apoplastic) and cell-to-cell (symplastic or transcellular) pathways running across peripheral cell layers (epidermis, cortex, endodermis) down to the xylem. Transcellular water transport is mediated in large part by aquaporin (AQP) water channels (Maurel *et al.*, 2015). Axial transport consists of conveying sap flow along xylem vessels, throughout the whole root system architecture (RAS), up to the aerial parts (Gambetta et al., 2017). The conductance of the radial and axial pathways can be altered in response to multiple environmental cues, providing a continuous adjustment of root hydraulics to water availability and demand (Aroca *et al.*, 2011; Boursiac *et al.*, 2022b). In particular, water deprivation can lead to rapid changes in AQP activity (Hachez et al., 2012;). These effects which depend on drought intensity can result, depending on genetic background, in a monotonous inhibition of root hydraulic conductivity (Lp_r) or in bell-shaped dose-response curves (Rosales et al., 2019). On the longer term, WD can also alter xylem development with contrasting effects depending on species (Ramachandran et al., 2020). Finally, WD enhances suberization of both exo- and endodermis, possibly altering solute transport (Doblas et al., 2017).

In recent years, efforts have been made to assess the radial and axial water transport properties of plant roots, using a combination of experimental and mathematical modeling approaches on excised segments or whole root systems (Boursiac *et al.*, 2022a; Heymans *et al.*, 2021; Meunier *et al.*, 2018; Zarebanadkouki *et al.*, 2016). Most recent works rely on hydraulic models imbedded within RSA, based on the Hydraulic Tree Model of Doussan et al. (Boursiac *et al.*, 2022a; Doussan *et al.*, 1998a; Doussan *et al.*, 1998b; Meunier *et al.*, 2017; Zarebanadkouki *et al.*, 2016), or on approaches that combine a hydraulic cross-sectional model at cellular level with anatomical observations along the root (Couvreur *et al.*, 2018; Ding *et al.*, 2020; Heymans *et al.*, 2021).

More integrative root models that couple water and solute transport have also been existing for decades. The first models were based on a representation of the root as an osmometer. The whole root system was reduced to one, two or even three membranes separating homogeneous compartments (Fiscus, 1975, 1977, 1986; Miller, 1985b; Murphy, 2000; Steudle, 1994). Some more recent models provide a longitudinal, bi-dimensional representation of unbranched root structures considering the role and transport selectivity of Casparian strips and suberin lamellae (Foster and Miklavcic, 2016, 2017). Complementary to these, (Couvreur *et al.*, 2018) proposed a 2D cross-sectional model computing water transport at subcellular levels (walls, membranes, and plasmodesmata) and considering apoplastic solute diffusion and symplastic homeostasis.

Hydraulic models at RSA level are designed to account for the non-uniformity of hydraulic parameters like axial conductance. Therefore, they can efficiently simulate the heterogeneity, over the whole root system, of radial and axial hydraulic flows and of water potential components (e.g. hydrostatic pressure in the xylem). However, none of these models has been able to simulate whole

Accepted Manuscript

Downloaded from https://academic.oup.com/jxb/advance-article/doi/10.1093/jxb/erac471/6896019 by guest on 02 January 2023

root water transport under WD conditions, when osmotic driving forces become predominant. Current root osmometer models can do so but, conversely, cannot represent the heterogeneous aspects of a RSA since the root is modeled as a restricted number of compartments in which solute concentration is homogeneous and pressure is uniform. Interestingly, these models have been able to mimic to a certain extent some experimental and puzzling observations like the non-linear relation between sap flow and pressure (Steudle, 1994). Integrating water and solute transport models within RSA could therefore provide a means to account for all the pre-cited aspects and, ultimately, investigate the multiple effects of WD on root water and solute transport parameters.

Boursiac et al. recently proposed an inverse modeling approach, based on pressure chamber measurements in excised roots, to simultaneously assess axial conductance and radial conductivity of complex branched root structures (Boursiac *et al.*, 2022a). This approach, called cut-and-flow, consists in measuring exuding sap flow rate, at a constant working pressure, in a root system that is successively cut from its distal part. A Hydraulic Tree Model named HydroRoot (DOI: 10.5281/zenodo.6584200) was inverted to fit the cut-and-flow data, thereby allowing a determination of the axial conductance profile and radial conductivity on the same root system. Because it exclusively considers hydrostatic driving forces, this model cannot operate in roots under WD or when osmotic forces are predominant.

To fill this gap and describe the concomitant transport of water and solutes in roots under WD, we coupled within realistic RSAs of maize seedlings a hydraulic model to a solute transport model of Fiscus' type (Fiscus, 1977). Cut-and-flow data and pressure-to flow relationships ($J_v(P)$) were used in an inverse modeling approach to determine the radial and axial hydraulic conductivities of primary roots grown under standard or WD conditions. This approach allows to resolve dramatic effects of WD on both radial and axial conductivities.

Materials and Methods

Plant material, growth and experimental conditions

Seeds of a maize B73-UH007 hybrid (B73H) (Millet *et al.*, 2016) were surface-sterilized in 50 ml of 1.4% bleach with a drop (~ 50 µL) of Tween-20 for 15 min under gentle agitation. The seeds were then treated with 35% H_2O_2 for 2 min, rinsed with 70% ethanol, and washed 6 times with sterilized water. The seeds were overlaid with wet clay beads in a plastic box, which was itself covered by a transparent plastic film. Seeds were germinated in the dark and further grown in a growth chamber at 65% relative humidity, with 22°C/20°C and 15 h/9 h light/dark cycles (150 $\mu E.m^{-2}.s^{-1}$).

At five days after sawing (DAS), seedlings were transferred to a hydroponic container filled with 24 L of a medium containing 1.25mM KNO_3, 0.75mM $MgSO_4$, 1.5mM $Ca(NO_3)_2$, 0.5mM KH_2PO_4, 0.1mM $MgCl_2$, 0.05mM Fe-EDTA, 0.05mM H_3BO_3, 0.012mM $MnSO_4$, 0.7mM $CuSO_4$, 0.001mM $ZnSO_4$, 24.10^{-5} mM MoO_4Na_2, 1.10^{-5} mM $CoCl_2$, 0.1mM Na_2SiO_3, and 1mM MES. Plants were grown in this solution for two days. At seven DAS, seedlings were transferred for four additional days to a fresh medium containing 150 g/L of high molecular weight polyethylene glycol (PEG-8000) to reduce the water potential of the nutrient solution. The control plants were transferred for four days in a fresh hydroponic solution. The water potential of the control hydroponic solution (-0.034 MPa) was measured with a WESCOR 5520 vapor pressure, with a resolution of 1 mmol/kg ($2.5\ 10^{-3}$ MPa at 293 °K). Addition of 150 g/L PEG to the control solution leads to a final water potential of - MPa,

Accepted Manuscript

Downloaded from https://academic.oup.com/jxb/advance-article/doi/10.1093/jxb/erac471/6896019 by guest on 02 January 2023

according to the empiric law used to determine the water potential of PEG solution (see below the paragraph Viscosity and water potential of a PEG solution).

Overall, two bathing solutions were used for plant growth and pressure chamber experiments: the control (CTR) hydroponic solution and the hydroponic solution containing 150 g/L PEG (PEG). This resulted in three plant sets:

(i) eight CTR plants, grown in a CTR hydroponic solution, with measurements done in the same solution (ii) eight PEG plants grown in a PEG hydroponic solution, with measurements done in the same solution (iii) five PEG-CTR plants grown in a PEG hydroponic solution, and transferred into a CTR solution for one hour prior to water transport measurements in the same CTR solution.

Measurements of pressure-dependent xylem sap flow [$J_v(P)$]

Root water flow was measured on de-topped primary roots using a set of pressure chambers with automated recording as described in (Boursiac *et al.*, 2022a). The primary root was carefully excised below the grain, placed into an adapter sealed with dental paste (Coltene Whaledent, France) and threaded across the silicone seal of the pressure chamber lid. The root was then placed into the pressure chamber in a container filled with either a CTR or PEG hydroponic solution. The adapter was connected to a flowmeter (Bronkhorst, France) in order to record the flow of sap (J_v) from the root system at successive pressures (P) applied on the bathing solution using nitrogen gas. Typical successive relative pressure steps were, in MPa: 0.00, 0.05, 0.15, 0.10, 0.25, 0.20, 0.35, 0.30, 0.45, 0.50, 0.25, 0.00. (0.00 represents the atmospheric pressure). Some experimental data sets comprise fewer pressure steps, down to 4 including exudation at atmospheric pressure. Only 4 plants over 21 had less than 6 steps.

To estimate the deviation of a measured or adjusted $J_v(P)$ relationship from a linear response to pressure, we normalized between 0 and 1 the fluxes and pressures according to their minima and maxima. This allows to compare roots that have very disparate fluxes in absolute values. We then quantified the gap to linearity by the maximal residual between the $J_v(P)$ relationship and the bisector.

Cut-and-flow experiment

Cut-and-flow measurements were performed just after $J_v(P)$ measurements. The operating pressure was set constant over the whole experiment: 0.3 MPa with PEG solution and 0.2 MPa with CTR solution (unless for two plants done at 0.3 MPa as well). In brief, and along the lines of our previous work (Boursiac *et al.*, 2022a), J_v was first recorded in the intact root system at the operating pressure. The root was taken out of the chamber and placed in a petri dish filled with their bathing solution. The lateral roots were stretched and aligned along the primary root and the whole root system was cut with a razor blade at a given distance to the tip, typically a few centimeters. Leaving the cut root segments in the petri dish, the remaining part of the root system was placed back into the chamber at the operating pressure and the J_v was recorded. This procedure was repeated successively.

To be as fast as possible during the cutting process (average cutting time was 140 ± 8 s), the cut length between successive excisions was approximate. Overall, the first cuts were 8.3 ± 0.6 cm on

Accepted Manuscript

Downloaded from https://academic.oup.com/jxb/advance-article/doi/10.1093/jxb/erac471/6896019 by guest on 02 January 2023

average whereas the mean length of subsequent cuts was 4.3 ± 0.2 cm and the average length of the remaining root system was 5.2 ± 0.6 cm.

Digitizing of root architectures

The root segments released after each cut and the basal root system remaining after the last cut were scanned at 600 dpi. The root parts were then digitized using SmartRoot (Lobet *et al.*, 2011), an ImageJ plugin, the segment lengths and the lateral position on their parent root were exported as text file in csv format. The complete root system was then reconstructed by recognizing, at each cut, the segments belonging to the primary root and the ones belonging to the laterals, and by pasting them to the remaining system. For example, considering an experiment with n successive cuts, the segments from the last cut were pasted to the remaining basal root system. Then the segments from the previous cut (n-1) were pasted to this new basal root system, and so on. Note that we did not scan the intact root system to avoid any damage before measurements.

The diameters of the primary root and its laterals were entered into the model for building the representation of the RSA (see Water and solute transport model). They were determined from three independent panels of CTR and PEG plants. Each experiment had six to ten plants of each type, yielding a final count of 23 CTR and 28 PEG plants. The roots were scanned, and the diameters were estimated using ImageJ. The average primary root diameters were 1.05 mm (n=104) and 1.03 mm (n=133) for CTR and PEG plants, respectively, with standard errors in the range of $2\ 10^{-3}$ mm. The average lateral root diameters were 0.36 mm (n=1345) and 0.39 mm (n=1495) for CTR and PEG plants, respectively, with standard errors below $2\ 10^{-4}$ mm. The 11-day-old roots had only first order laterals.

Water and solute transport model

The present model is a modification of the HydroRoot RSA hydraulic model (Boursiac *et al.*, 2022a). HydroRoot was developed as a component of the OpenAlea platform (Pradal *et al.*, 2008). It uses a Multiscale Tree Graph (MTG) (Godin and Caraglio, 1998) to represent a root hydraulic architecture, which consists of the topology of a root system (branching positions, root lengths, root radii, etc.) and its hydraulic structure (local radial and axial conductivities). With respect to (Boursiac *et al.*, 2022a), the main modification of HydroRoot was the addition of solute transport equations to the hydraulic model. This change led to a major difference in the resolution of the equation system on the whole RSA. Thus, the hydraulic architecture can no longer be modeled by an analogous electrical network (Boursiac *et al.*, 2022a) and the coupled solute and water transport equations had to be solved in a matrix form.

The model was developed at millimetric scale, the order of magnitude of the primary root diameter. The RSA was discretized in cylindrical elementary volumes (Figure 1), considered as representative elementary volumes (REV). The REV diameter, d, is equal to the root diameter, and depends on the root order (primary or first laterals). The REV length, l, is of the order of the diameter, here 1 mm, which was small enough to get numerical convergence. The local transport equations described below were considered in each REV. Each REV can be seen as two concentric media: the peripheral tissues (from epidermis to pericycle) through which radial transport happens, and a central medium (stele with xylem vessels) where the sap flows axially. In the following, the parameter units are displayed within brackets and correspond to the international system of units.

Accepted Manuscript

Downloaded from https://academic.oup.com/jxb/advance-article/doi/10.1093/jxb/erac471/6896019 by guest on 02 January 2023

Water transport

The hydraulic model is the same as in HydroRoot, with the addition of a radial water flow rate due to osmotic potential difference. Thus, the radial water flux can be modeled as follows:

$$j = k\left(\Delta\Psi_{\mathrm{H}} + \Delta\Psi_{\mathrm{peg}} + \sigma\Delta\Psi_{S}\right)S \quad (1)$$

where j is the local radial water flow rate, k (m.s^{-1}.MPa^{-1}) the radial hydraulic conductivity. $\Delta\Psi_{\mathrm{H}}$, $\Delta\Psi_{\mathrm{peg}}$ and $\Delta\Psi_{S}$ (MPa) correspond to the hydrostatic water potential difference between the bathing solution and the xylem sap, to the osmotic water potential difference due to the PEG and to the osmotic water potential difference due to the solutes, respectively. σ is the effective reflection coefficient. S ($S = \pi\, d\, l$) is the external surface area of the REV (m²). Expressing the water potentials, equation (1) can be written as follows:

$$j = k\left(P_e - P - \pi_{\mathrm{peg}}^{\mathrm{ext}} + \pi_{\mathrm{peg}} - \sigma RT(C_e - C)\right)S \quad (2)$$

where P_e and P are the hydrostatic pressure of the bathing solution and within the xylem vessels, respectively, $\pi_{\mathrm{peg}}^{\mathrm{ext}}$ and π_{peg} the PEG contribution to the osmotic pressure of the bathing solution and inside the xylem vessels, respectively, C_e and C the solute concentration in the bathing solution and in the xylem vessels (mol.m^{-3}),respectively, R the gas constant, T the temperature (set to 298°K here). Both $\pi_{\mathrm{peg}}^{\mathrm{ext}}$ and π_{peg} are calculated according to PEG concentration (Supplementary Fig. S1A). Since PEG 8000 is a non-permeant solute, its contribution to the osmotic pressure inside the xylem (π_{peg}) is only considered in cut-and-flow experiments within PEG bathing solutions.

The axial sap flow rate was modeled with a Hagen-Poiseuille's law type:

$$J = K(\mu)\frac{\Delta P}{l} \quad (3)$$

where J is the axial sap flow rate, $K(\mu)$ the axial conductance that depends on sap viscosity (m^4.s^{-1}.MPa^{-1}; see below), ΔP the local pressure difference between two REVs, l the length of the REV. The axial conductance is inversely proportional to the fluid viscosity μ, as illustrated for example by the conductance in a cylindrical capillary of radius r: $K(\mu) = \pi r^4/(8\mu)$. The sap is commonly considered having water viscosity. Thus, axial conductances were displayed as corresponding to a sap viscosity of 1 mPa.s (equation (3)) and not independently of the viscosity, as follows: $J = (K/\mu)\,(\Delta P/l)$ .The former expression is commonly used in the literature (Doussan et al., 1998a; Doussan et al., 1998b; Heymans et al., 2021; Landsberg and Fowkes, 1978; Meunier et al., 2018; Zarebanadkouki et al., 2016) and allows better comparisons. Note, however, that when PEG penetrates the root vasculature in cut-and-flow experiments, the viscosity significantly increases with the PEG concentration (see next paragraph) and has to be taken into account.

To reduce the number of parameters to be adjusted (see Parameter determination), σ was set to 0.85, a value reported for nutrients on maize root systems (Miller, 1985a). Sensitivity tests were done to evaluate the impact of σ on the other parameters (see Results and Discussion).

Accepted Manuscript

Downloaded from https://academic.oup.com/jxb/advance-article/doi/10.1093/jxb/erac471/6896019 by guest on 02 January 2023

Solute transport

The modeling of solute transport is based on two experimental observations: exudation at atmospheric pressure and negative sap flow observed in some PEG roots. Under atmospheric pressure monitoring, sap flow is driven by the osmotic pressure gradient due to the solute concentration difference between the outer solution and xylem sap (see equation (2)). Pure hydraulic models, without any solute transport to the xylem vessels, cannot explain such behavior in steady state. To account for a constant positive exudation rate, the solutes exiting the root by exudation must indeed be balanced by an uptake of solutes. Thus, in addition to the water radial flux, we hypothesized a constant active uptake rate of solutes, noted J_s^* after Fiscus (Fiscus, 1975). Yet, the steady and negative sap flow rate observed in some PEG roots raises specific questions. If sap continuously flows from the root base to the bathing solution, whereas solutes driven by J_s^* keep entering the root at a constant rate, the solute concentration in xylem vessels should increase indefinitely, in contradiction with the mass balance principle that should be verified in any REV of the root. Therefore, an additional solute flux, or leakage, from the xylem vessels to root bathing solution, was modeled as a passive diffusion characterized by the tissue permeability P_s. The radial solute flux was therefore expressed as follows:

$$j_s = [J_s^* - P_s(C - C_e)]S \tag{4}$$

where j_s (mol.s^{-1}) is the radial solute flux, J_s^* (mol.m^{-2}.s^{-1}) is the solute active uptake rate and P_s (m.s^{-1}) is the radial permeability of the root peripheral tissues. As in equation (2), C and C^e correspond to the solute concentration in the xylem vessels and in the bathing solution, respectively. S is the external surface area of the REV.

Since solutes are transported along xylem vessels by advection, axial solute flux can be expressed as $J_s = JC$ (mol.s^{-1}). When PEG penetrates the root in cut-and-flow experiments, its axial flux has the same form: $J_{\mathrm{peg}} = JC_{\mathrm{peg}}$ (mol.s^{-1}) where C_{peg} is the PEG concentration in the xylem vessels. Details about the discretization of the equations and their resolution on the matrix form of the RSA can be found in Supplementary Protocol S1.

The overall coupled model of solute and water transport within a RSA is summarized in Figure 1. The subfigure C sketches a case where the hydrostatic pressure of the bathing solution is greater than the atmospheric pressure at the basal part of the root, and the outer concentration of solutes is lower than the sap one. Added to the radial water flux, the two solute transport components (J_s^*, P_s) are also represented.

Viscosity and water potential of a PEG solution

The water potential of a PEG solution, Ψ_{peg}, does not follow the Van't Hoff's law but can be described, at a given temperature, by an empirical polynomial law (see equation 1 in (Michel, 1983) and Supplementary Fig. S1 A). The osmotic pressure of PEG solution can be expressed as $\pi_{\mathrm{peg}} = -\Psi_{\mathrm{peg}}$. For a PEG concentration of 150 g/L, Ψ_{peg} = -0.302 MPa.

To consider the viscosity (μ) of a PEG solution (Supplementary Fig. S1 B), we used the following law:

$$\mu(w_{\mathrm{peg}}) = -17.4 + 18.4 \exp\left(\frac{w_{\mathrm{peg}}}{0.279}\right)$$

Accepted Manuscript

Downloaded from https://academic.oup.com/jxb/advance-article/doi/10.1093/jxb/erac471/6896019 by guest on 02 January 2023

which derives from a fit done on data from (Gonzalez-Tello *et al.*, 1994) for w_{peg} between 100 and 200 g/L, with a data point (1 mPa.s) added at w_{peg}=0 to integrate the viscosity of pure water. Note that a PEG solution at 150 g/L exhibits a viscosity of 14 mPa.s while water viscosity is 1 mPa.s.

Parameter determination

The principle is to adjust the axial conductance (*K*) profile, the radial hydraulic conductivity (*k*), the active solute uptake (J_s^*) and the solute permeability (P_s) to get the best fit on both J_v(P) and cut-and-flow experiments. The fit is obtained by minimizing the objective function *F* set as the sum of the squared errors, $F = \Sigma(J_v - J)^2$, J_v being the experimental data and J the simulated ones.

The axial conductance is known to vary with the distance to root tip (Boursiac *et al.*, 2022a; Doussan *et al.*, 1998b; Frensch and Steudle, 1989; Heymans *et al.*, 2021; Meunier *et al.*, 2018; Zarebanadkouki *et al.*, 2016). The *K* profile was therefore represented as a linear piecewise function of the distance to root tip. The number of points and their abscissa were the number of cuts and their distance to tip, respectively. Thus, the function was different between plants, with up to 9 points. Since *k*, J_s^* and P_s are uniform, the maximum number of parameters was 12.

The parameter first guesses used to start the adjustment were:

(i) an axial conductance profile derived from the tap root profile of (Heymans *et al.*, 2021). This profile corresponds to a step function with K_{min}=10^{-12} and K_{max}=10^{-10} $m^4.MPa^{-1}.s^{-1}$. The step was positioned at around 0.1 m depending on the abscissa of the cut-and-flow data.

(ii) a radial conductivity equal to 10^{-7} $m.MPa^{-1}.s^{-1}$. This arbitrary value is consistent with literature reports from 0.5-1.5 10^{-7} $MPa^{-1}.s^{-1}$ (Heymans *et al.*, 2021) to 2.5 10^{-7} $m.MPa^{-1}.s^{-1}$ (Frensch and Steudle, 1989).

(iii) J_s^*=10^{-7} $mol.m^{-2}.s^{-1}$ and P_s=$10^{-9}$$m.s^{-1}$. Such orders of magnitude can be found in literature for maize or *Phaseolus* roots (Birner and Steudle, 1993; Fiscus, 1986; Steudle and Brinckmann, 1989).

We used the optimize.minimize function of the SciPy Python library (Virtanen *et al.*, 2020) to perform these minimizations. Local optimization routines were used because global optimizations, such as dual annealing, were often unable to get a correct fit. Due to the heterogeneity of the plants and condition panel, an identical numerical workflow was sometimes not possible. Thus, we used different optimization routines, running several times the optimization process. The main workflow was:

(i) to start from the first guesses with the adjustment of *K* and *k* on the cut-and-flow data without any solute transport using the workflow of (Boursiac *et al.*, 2022a).

(ii) to keep the *K* obtained in (i), adjusting *k*, J_s^* and P_s on the J_v(P) data. Here, the solver of optimize.minimize that was mainly used was Sequential Least Squares Programming (SLSQP).

(iii) to finalize with the adjustment of all the parameters on J_v(P) and cut-and-flow data. Here, the solver that was mainly used was Constrained Optimization BY Linear Approximation (COBYLA).

Accepted Manuscript

Downloaded from https://academic.oup.com/jxb/advance-article/doi/10.1093/jxb/erac471/6896019 by guest on 02 January 2023

Results

$J_v(P)$ and cut-and-flow experiments in roots under control and WD conditions

Focusing on functional responses of maize primary roots to WD, the pressure chamber technique was used to measure the flow-to-pressure relationship [$J_v(P)$] and obtain cut-and-flow data in de-topped roots. WD was induced by addition of PEG-8000 (150 g/L), lowering the water potential of the bathing solution to -0.336 MPa. Three different sets of growth and experimental conditions were used. Control (CTR) plants were grown in a standard hydroponic solution and de-topped roots were studied in the same solution. PEG plants were exposed to WD for 5 d with water transport measurements done in the same PEG bathing solution. PEG-CTR roots were derived from plants grown in a PEG solution and transferred into a control solution for one hour prior to pressure chamber measurements in a control solution. Besides methodological considerations, the latter treatment allows to explore the reversibility of WD effects on root water transport parameters.

Figure 2 shows six examples of $J_v(P)$ relationships measured in the three series of roots. PEG roots (Figure 2 C and D) showed non-linear curves, a properties observed in six out of eight plants. In contrast, $J_v(P)$ curves of the two other root types (CTR or PEG-CTR) were more linear. Yet, two of these roots (Figure 2 A and F) showed a weak non-linearity below 0.1 MPa. Another key property emphasized by Figure 2 D is the possible occurrence of negative xylem flow rates for positive hydrostatic pressure differences, up to 0.2 MPa. This is also shown in Figure 3, which displays xylem flow rates at atmospheric pressure [$J_0=J_v(0)$], i.e. without any external hydrostatic driving force. These flow rates are very stable over time and could be measured in some roots for up to one hour. For the eight PEG roots, the average J_0 was $-2.5 \pm 0.9\ 10^{-3}$ $\mu L.s^{-1}$. By contrast, roots bathing in a control hydroponic solution yielded positive J_0 values (CTR: $J_0 = 2.1 \pm 0.8\ 10^{-2}$ $\mu L.s^{-1}$; PEG-CTR: $J_0 = 1.4 \pm 0.6\ 10^{-2}$ $\mu L.s^{-1}$) (Figure 3).

Figure 4 is the counterpart of Figure 2. It refers to the same individual roots, showing corresponding cut-and-flow experiments performed after $J_v(P)$ measurements (Figure 2). In brief, Figure 4 shows increases in pressure-induced flow rate upon progressive cuts of the root system from root tips to base. The curves determined in CTR roots are characterized by a low initial slope that increases with length of the cut root (Figure 4 A and B). The four other curves, derived from PEG and PEG-CTR roots, show a less convex shape, with higher slopes from the first cut. Thus, the cut-and-flow curves catch the impact on root functional properties of plant growth under WD.

The same conclusions can be drawn from $J_v(P)$ and cut-and-flow data obtained in a total of 15 additional CTR, PEG or PEG-CTR roots (Supplemental Figures 2, 3 and 4).

Integration of solute and water flows throughout RSA

Based on the experimental data documented above, we developed a RSA model of water and solute transport allowing to fit the $J_v(P)$ and cut-and-flow data of roots exposed to control or WD conditions (Figures 2 and 4; Supplemental Figures 2, 3 and 4). Indeed, a pure water transport model could not explain exudation at atmospheric pressure or negative fluxes observed in some PEG roots. Basically, an osmotic term was added to the radial water flux (equation 1 and 2) and solute transport was coupled to hydraulic flow. Using the model within realistic RSA allowed to map the heterogeneity of solute and water flows throughout the root. Figure 5 shows representative CTR (Figure 5A-C) and PEG (Figure 5D-F) roots bathing in a CTR or PEG solution, respectively, under a same hydrostatic

Accepted Manuscript

Downloaded from https://academic.oup.com/jxb/advance-article/doi/10.1093/jxb/erac471/6896019 by guest on 02 January 2023

overpressure of 0.1 MPa. Note that, as indicated below, the hydraulic and solute transport parameters were determined by fitting J_v(P) and cut and flow data (Figure 2A and 2C; Figure 4A and 4C). For each root, the figure depicts the heat map of the hydrostatic and osmotic driving components (see equation (2)), $\Delta P = P_e - P$ and $\Delta C = C - C_e$, and the resulting local radial water fluxes. The CTR root shows an increasing Δ*P* from the tips to the base with a negative difference at the primary tip that would drive a radial efflux of water (Figure 5 A). Yet, influxes occur throughout the RSA (Figure 5C), indicating that the dominating force driving water influx in the primary tip is ΔC (Figure 5 B). In addition, a progressive drop in xylem solute concentration is observed along the RSA, due to dilution effects by the sap flow. Thus, the progressive increase in radial flows along the RSA can be explained by a dominating effects of variations in ΔP over variations in ΔC (Figure 5 C). Although the PEG root is bathing in a medium with a low osmotic potential (-0.336 MPa), it presents the same trends as the CTR root, with water influxes throughout the RSA, a progressive increase of Δ*P* from the tips to the base and, inversely, a progressive drop of Δ*C* (Figure 5 D-F). Whereas radial water influx varies in parallel to ΔP variation, as in the CTR root, the absolute value of Δ*P* remains in the range of 0.1 MPa which is insufficient to counter balance the external water potential of -0.336 MPa. Therefore, both ΔP and ΔC serve as joint driving forces. Finally, we note that, although the PEG root harbors gradient properties throughout its architecture, these variations are of very low amplitude (< 1%), much lower than in the CTR root ($-0.085 < \Delta P < 0.100$ (MPa); $-1.7 < \Delta C < 46.6$ (Mol.m^{-3})). Therefore, the PEG root has much more homogeneous properties inside the xylem vessels than the CTR root.

Figure 6 shows the heat maps of Δ*P*, Δ*C* and local radial fluxes in a representative CTR root, but under spontaneous exudation condition. A water influx can be observed throughout the RSA (Figure 6C). Yet, a negative Δ*P* can be observed over the whole architecture, with an increasing value to the base (Figure 6A). Such Δ*P*, which counteracts radial water inflow, is due to the induction of a sap flow in the xylem. As discussed above, the Δ*C* decrease to the tips results from dilution effects due to water flow (Figure 6B). Therefore, the major driving force for radial influx is Δ*C*, and its variation along the RSA is concomitantly controlled by Δ*P* and Δ*C*.

These few examples illustrate the capacity of the present modeling approach to resolve how integration throughout a RSA of discretized elementary modules leads to heterogeneity in driving forces and elementary flows, depending both on root type and water transport mode.

Axial conductance profiles of roots under standard and WD conditions.

The present approach was further used to obtain a comprehensive view, using model inversion, of the water and solute transport properties of real roots, obtained from CTR or PEG plants, and measured in CTR or PEG solutions. Here again, parameter adjustments were done concomitantly on the J_v(P) and cut-and-flow data, taking into account penetration of PEG in xylem vessels during cut-and-flow experiments. One set of parameters was therefore obtained for each of 21 roots investigated. Best fits of these experiments are shown in Figure 2, Figure 4 and Supplemental Figures 2, 3 and 4. We note that, for all roots investigated, the goodness of fit (R^2) for the relationship between the measures and values simulated from the fitted model was higher than 0.91 (Supplementary Fig. S5).

Accepted Manuscript

Downloaded from https://academic.oup.com/jxb/advance-article/doi/10.1093/jxb/erac471/6896019 by guest on 02 January 2023

Figure 7 shows the axial conductance (*K*) profiles obtained by Locally Weighted Scatterplot Smoothing (lowess) of CTR (n=8), PEG (n=8) and PEG-CTR (n=5) data sets. The *K* profiles of roots grown in the presence of PEG, whatever the J_v(P) measuring solution (PEG or CTR), are very close to each other. Since measurements in PEG-CTR roots were performed one hour after their transfer into a CTR solution, we assume that their xylem anatomy (and therefore their *K* profile) was similar to that of PEG roots. Thus, these results indicate that the bathing solution used during the cut-and-flow experiment, and in particular the presence or absence of PEG, does not interfere with the determination of *K*. As a consequence, our approach reveals, with respect to CTR roots, a dramatic increase of *K* in root tips grown under WD.

Determination of radial hydraulic conductivity and solute transport parameters

Figure 8 shows the distribution of the three radial transport parameters giving the best fits. With respect to CTR roots, PEG roots showed a tenfold decrease in mean radial hydraulic conductivity (*k*). This result is in accordance with the decrease in hydraulic conductivity commonly observed in roots under WD (Steudle, 2000b), such as in Arabidopsis grown in a 150 g/L PEG solution (Rosales *et al.*, 2019). PEG-CTR roots showed *k* values similar to those of CTR roots pointing to a quick reversal of the WD-induced inhibition of *k*. The solute transport parameters (J_s^*, P_s) were more difficult to interpret with respect to known effects of WD. This difficulty was reflected by the fact that the CTR and PEG-CTR data were very scattered.

Sensitivity analysis of the model

To possibly understand the scattering of J_s^* and P_s inferred values, we investigated the sensitivity of adjusted *k* to the two solute transport parameters. In the following, we note k_0, J_{s0}^* and P_{s0} the parameter values giving the best fit. The test was run for the CTR and PEG roots corresponding to panels A and C of Figure 2, respectively. It consisted in adjusting *k* on J_v(P) for various values of J_s^* and P_s and to look at the range of J_s^* and P_s variations for a 10% change of *k* around k_0. For the CTR root, a ±10 % variation of the adjusted *k* was obtained for J_s varying from 5 10^{-4} to 4 times J_{s0} and for P_s varying from 5 10^{-4} to 131 times P_{s0}. The objective function (*F*) was almost multiplied by 10, varying from its minimum 2.6 10^{-4} to 2.2 10^{-3}. In the PEG root, a ±10 % change of the adjusted *k* was obtained for J_s varying from 4 10^{-4} to 2.05 times J_{s0} and for P_s varying from 1 10^{-3} to 4.0 times P_{s0} with *F* varying by two orders of magnitude from its minimums. Thus, in either type of roots, the determination of radial hydraulic conductivity *k* shows low sensitivity to the active uptake rate and the passive permeability of solutes.

In the present model, the reflection coefficient (σ) was initially set to 0.85, a value previously reported for nutrients in maize root systems (Miller, 1985a). In order to evaluate the impact of σ on determination of other parameters, we performed two sets of adjustment, with two contrasting values, σ = 1 and σ = 0.5, respectively. With respect to axial conductance profiles determined with σ = 0.85, the maximum discrepancy was obtained for CTR roots and σ = 1, with an average change of *K* of 1.2%. In all the other cases, *K* variations were lower than 1%. Determination of *k* was also largely insensitive to σ with a maximum change of mean *k* below 3% (Supplementary Fig. S6 A and D). For the two other parameters, P_s and J_s^*, the results were more contrasted (Supplementary Fig. S6 B, C, E and F). In CTR and PEG roots, mean J_s^* and P_s could increase by up to 25% (σ = 0.5). In PEG-CTR roots, mean J_s^* and P_s were increased by up to 40% and 6%, respectively, for σ = 0.5.

Accepted Manuscript

Downloaded from https://academic.oup.com/jxb/advance-article/doi/10.1093/jxb/erac471/6896019 by guest on 02 January 2023

These analyses assess the accuracy with which effects of WD on root hydraulic parameters can be determined using the present inverse modeling approach.

Discussion

In the present work, we developed a model of root hydraulic architecture aimed at describing the behavior of maize primary roots under control or WD conditions. Besides radial and axial water transport, that were represented using a fairly classical Hydraulic Tree Model, solute transport was also considered throughout RSA, using both an active uptake rate and a tissue permeability coefficient. As in our earlier work (Boursiac *et al.*, 2022a), our main aim was to develop an inverse modeling approach to assess the radial conductivity and the axial conductance profile of a branched root system. Yet, this procedure was improved as it relied not only on sap flow data obtained in cut-and-flow experiments but also on extensive $J_v(P)$ data obtained in intact roots. Most importantly, this procedure was validated in plants grown under standard conditions or PEG-induced WD. We showed that the solute transport must be considered to explain sap exudation at atmospheric pressure, when the driving force is essentially osmotic. Solute transport also allows to fit the specific features of the $J_v(P)$ data of some plants under WD with a non-linear relationship and negative sap fluxes. The experiments performed in different conditions demonstrated the robustness of the method to determine concomitantly the radial and axial water transport parameters on real RSA. Most importantly, they allowed us to obtain a comprehensive view of combined effects of WD on radial and axial hydraulic conductances.

The $J_v(P)$ curve shape

The $J_v(P)$ data reported in the present work showed two key properties: negative sap flow rates specific to PEG roots, and a non-linearity that was particularly accentuated in PEG roots. A non-linearity of sap flow according to applied pressure has already been described in maize (Gorska *et al.*, 2008; Miller, 1985b) or other plant species (Fiscus, 1986; Jackson et al., 1996; Markhart and Smit, 1990; Rüdinger et al., 1994). For instance, Miller (Miller, 1985b) reported $J_v(P)$ curves that were linear for positive relative pressures but showed a non-linear shape at negative relative pressures. Gorska *et al.* (Gorska *et al.*, 2008) observed that the $J_v(P)$ relationship can be considered as linear only for pressure above 0.1 MPa. These reports are in accordance with our measurements in roots bathing in a CTR solution, whatever the plant growth conditions (CTR or PEG). For roots grown and maintained under WD, we found the non-linearity to be further accentuated. This can be explained by the dramatically reduced radial conductivity of these roots (Figure 8 A). Since the non-linearity of $J_v(P)$ results from the changing balance between hydrostatic and osmotic driving forces, the reduced radial conductivity shifts to higher positive pressures the range at which the hydrostatic forces become preponderant and $J_v(P)$ linear.

Yet, the non-linearity of $J_v(P)$ cannot be modeled without considering solute transport. An absence of solute fluxes would imply that the osmotic pressure term in equation (2) is uniform over the RSA, leading to a linear relation. In fact, when $J_v(P)$ is monitored at high flow rates, this function can reasonably be adjusted with a linear fit. The slope can then be interpreted as the root hydraulic conductance, which yields the root hydraulic conductivity. In addition, the intercept with the pressure axis, P_0, is usually assumed to be the pressure needed to counter balance the osmotic pressure of the bathing solution (Passioura, 1988). To explore this further, we tried to determine *K*

Accepted Manuscript

Downloaded from https://academic.oup.com/jxb/advance-article/doi/10.1093/jxb/erac471/6896019 by guest on 02 January 2023

and *k* using such a purely hydraulic model, i.e. exclusively based on equations (2) and (3). In equation (2), the osmotic pressure term was set constant and equal to P_0 and therefore equation (2) was expressed as $j = k(P - P_0)S$, with *P* being the relative pressure. The fits were done on the linear part of $J_v(P)$ and on the cut-and-flow experiment. In CTR roots, *k* was found to be reduced by 9 % with respect to the value obtained with the water-solute transport model. The errors on *K* axial conductance profile were higher, up to 37 %. In PEG roots, the differences between the two model settings were higher, the averaged *k* being reduced by 21 % and *K* by up to 84 % when the osmotic pressure term was set to P_0. Thus, a simplified osmotic model which does not take solute transport into account results in significant variations in hydraulic parameter estimations. Supplementary Fig. S7 shows best fits of the experiments with a purely hydraulic model, and a constant osmotic pressure P_0. While the quality of fit with CTR roots is good ($R^2 = 0.95$), this type of model is unable to fit the PEG data at low pressure when the osmotic term is preponderant ($R^2 < 0.83$).

Development of a water/solute model at RSA level

Models that couple water and solute transport have been existing for decades, but they usually represent the whole root as a simplified osmometer with two or three compartments (Fiscus, 1975, 1977, 1986; Miller, 1985b; Steudle, 1994, 2000a). In these models, the root interior (i.e. the inner volume of the xylem vessels) is supposed to have a homogeneous solute concentration and hydrostatic pressure. Consequently, the water and solutes fluxes are uniform all over the root surface. This is, however, not the case in real root systems, where sap flow through axial resistances results in a hydrostatic pressure gradient along xylem vessels. This pressure gradient leads to a non-uniform pressure difference between the outer solution and the xylem vessels, that increases from the root tips (laterals and primary) to the basal ends (Figure 5 A and D; Figure 6A). The radial flow of water shows the same trend along the RSA (Figure 5 C and F; Figure 6C). Consequently, the sap flow rate increases towards the root base leading to a progressive decrease of the solute concentration (Figure 5 B and E, Figure 6B). In osmometer models, this dilution along the RSA is typically neglected. Consequently, these models overestimate the solute concentration inside the xylem compartment, leading to an overestimation of the flow rate. Indeed, $\Delta C = (C_e - C)$ decreases with increasing (overestimated) C, and as consequence $J = k(\Delta P - RT\Delta C)$ increases in these conditions.

To illustrate this point, we calculated an analytical solution of the present model, based on equations (2) and (4), for a root represented according to Fiscus (Fiscus, 1975, 1977) as a simple semipermeable barrier separating two compartments (see Supplementary Protocol S2). The comparisons of the adjusted transport parameters between the RSA model and the two-compartment model show marked differences for CTR and PEG-CTR roots (Supplementary Fig. S8). In particular, the radial conductivity *k* is significantly underestimated in the two-compartment model, by 65 % for CTR roots and 45 % for PEG-CTR roots. In contrast, the solute parameters, J_s^* and P_s, increase dramatically, by 77 and 78 %, respectively, for CTR roots, and by 84 and 88 %, respectively, for PEG-CTR roots. The water and solute transport parameters were noticeably less affected in PEG roots, with changes between 10 and 18 %. This is due to more homogeneous concentration profiles inside these roots because of lower fluxes. For instance, the difference in solute concentration, calculated from the basal end to the tip of the primary root, and divided by its length, was 92.7 ± 29.6, 2.3 ± 0.7 and 12.5 ± 3.0 $mol.m^{-4}$, for the CTR, PEG and PEG-CTR roots, respectively.

Accepted Manuscript

Downloaded from https://academic.oup.com/jxb/advance-article/doi/10.1093/jxb/erac471/6896019 by guest on 02 January 2023

Robustness of the cut-and-flow method to estimate axial conductance in roots under water deficit

As discussed above, the coupling of solute and water transport in the present root model prevented from significant errors in hydraulic parameter determination. In addition, the model had to represent the possible inflow of PEG in the root vasculature during cut-and-flow experiments. Effects of PEG on both radial osmotic potential differences and sap viscosity had to be modeled throughout RSA.

To assess these additional modeling constraints, we closely inspected the physiological consistency of data obtained in plants exposed to WD. In brief, both PEG-CTR and PEG plants were submitted to WD during their growth. Yet, the roots of the former plants were exposed to a CTR hydroponic solution for one hour prior to water transport experiments. By contrasts, roots of the latter plants were maintained in a PEG bathing solution during measurements. The axial conductance profiles *K* of the two series of roots were notably similar. In contrast, and in comparison to PEG roots, the radial conductivity of PEG-CTR roots was reversed to CTR root values. We believe this to be coherent, since *K* is linked to the xylem vessels that are fixed structures and probably cannot be altered significantly within one hour in a CTR solution. In contrast, *k* is related to aquaporin activity that can be reversed within this time lapse.

Whereas our results are in line with studies in numerous species showing WD-induced inhibition of aquaporin activity (Maurel et al., 2015; Rosales et al., 2019), they are at variance with the lack of effects of a PEG-induced WD on maize L_{pr}, as reported by Hachez et al. (2012). Future work will be required to determine to which extent differences in experimental conditions can account for this discrepancy. The precise description of effects of WD on axial conductance also represents a significant advance which will have to be related to effects of drought on root growth and/or xylem differentiation (Ramachandran et al., 2020). Note that the consistency of axial conductance determination would have not been achieved without considering in detail the viscosity of PEG-containing sap. To illustrate this, let us consider the Hagen-Poiseuille's law which predicts that the conductance of a pipe is inversely proportional to the fluid viscosity. Thus, the axial conductance of a pipe filled with a PEG solution at 150 g/L is 14 times lower than that of the same pipe filled with water (Supplementary Fig. S1B). Indeed, we checked that interpreting the cut-and-flow experiments done in a PEG bathing solution with a sap viscosity of 1 mPa.s leads to an underestimation of *K* by about an order of magnitude.

Reflection coefficient

In agreement with the idea that the maize root is permeable to solutes, we set σ to 0.85 in the present root functional model, a value reported in the literature for complete root systems bathing in a nutrient solution (i.e. the nature of the solutes is unknown and nutrients account for all solutes present in solution) (Miller, 1985a). Yet, we note that in few other works presenting reflection coefficient values for nutrients (non-differentiated solutes), σ was referenced close to unity (Fiscus, 1986; Knipfer *et al.*, 2021; Knipfer and Fricke, 2010). Nevertheless, we further tested the sensitivity of our model inversion method by performing parameter adjustments for σ = 1.0 and 0.5, 0.5 being the lower bound reported for solutes like sucrose in maize primary roots (Steudle, 2000a). Our results show that hydraulic parameters were essentially insensitive to σ, and that the two solute

Accepted Manuscript

Downloaded from https://academic.oup.com/jxb/advance-article/doi/10.1093/jxb/erac471/6896019 by guest on 02 January 2023

parameters were not strongly impacted (Supplementary Fig. S6). These considerations further support the robustness of the model inversion method.

Conclusion

In the present work, we have extended the toolbox developed by (Boursiac *et al.*, 2022a), combining experiment and modeling to assess the water and solute transport parameters of maize root systems under WD. The experimental data consisted of two successive measurement sets done with a pressure chamber: $J_v(P)$ determination, followed by a cut-and-flow experiment. A critical step was to formalize solute transport to account for the specific shape of the $J_v(P)$ curve of plants under WD. Furthermore, maize roots grown under WD were investigated under varying measurements conditions, thereby assessing the robustness of our inverse modeling approach. Thus, this novel procedure allows a concomitant determination of water and solute transport parameters and of their alteration upon exposure to WD. In brief, plants grown under WD exhibited, with respect to plants grown under standard conditions, a notable enhancement of axial conductance (K) in root tips. Conversely, the radial conductivity k was reduced tenfold upon direct exposure of roots to WD. Further studies will have to address more complex RSAs considering, for instance, specific hydraulic and solute transport properties in lateral roots and a non-uniform radial conductivity along the root axis. To do so, it may be useful to integrate in the present inverse modeling approach other experimental parameters such as solute concentration in the exuded sap. Finally, our approach can be extended to testing the effects of other environmental factors, such as hypoxia, on water and solute transport in roots.

Accepted Manuscript

Downloaded from https://academic.oup.com/jxb/advance-article/doi/10.1093/jxb/erac471/6896019 by guest on 02 January 2023

Acknowledgements

Author contributions

FB and CM conceived the study; FB performed all of the experiments with help from VP and advice from YB; FB developed the model and performed all formal analyses in interaction with YB, CP and CM; FB and CM wrote the manuscript which was checked by all authors.

Funding

This work was supported the European Research Council (ERC) under the European Union's Horizon 2020 research and innovation program (Grant Agreement ERC-2017-ADG-788553).

Conflict of Interest

The authors have no conflict of interest to declare.

Data Availability

The data supporting the findings of this study are available from the corresponding author, Christophe Maurel, upon request.

Accepted Manuscript

Downloaded from https://academic.oup.com/jxb/advance-article/doi/10.1093/jxb/erac471/6896019 by guest on 02 January 2023

Literature cited

Aroca R, Porcel R, Ruiz-Lozano JM. 2011. Regulation of root water uptake under abiotic stress conditions. Journal of Experimental Botany **63**, 43-57.

Birner TP, Steudle E. 1993. Effects of anaerobic conditions on water and solute relations, and on active transport in roots of maize (*Zea mays* L.). Planta **190**, 474–483.

Boursiac Y, Pradal C, Bauget F, Lucas M, Delivorias S, Godin C, Maurel C. 2022a. Phenotyping and modeling of root hydraulic architecture reveal critical determinants of axial water transport. Plant Physiology, doi: 10.1093/plphys/kiac1281. [Preprint].

Boursiac Y, Protto V, Rishmawi L, Maurel C. 2022b. Experimental and conceptual approches to root water transport. Plant and Soil **478**, 349-470.

Couvreur V, Faget M, Lobet G, Javaux M, Chaumont F, Draye X. 2018. Going with the Flow: Multiscale Insights into the Composite Nature of Water Transport in Roots. Plant Physiology **178**, 1689-1703.

Ding L, Milhiet T, Couvreur V, et al. 2020. Modification of the Expression of the Aquaporin ZmPIP2;5 Affects Water Relations and Plant Growth. Plant Physiology **182**, 2154-2165.

Doblas VG, Geldner N, Barberon M. 2017. The endodermis, a tightly controlled barrier for nutrients. Current Opinion in Plant Biology **39**, 136–143.

Doussan C, Pagès L, Vercambre G. 1998a. Modelling of the Hydraulic Architecture of Root Systems: An Integrated Approach to Water Absorption–Model Description. Annals of Botany **81**, 213–223.

Doussan C, Vercambre G, Pagè L. 1998b. Modelling of the Hydraulic Architecture of Root Systems: An Integrated Approach to Water Absorption—Distribution of Axial and Radial Conductances in Maize. Annals of Botany **81**, 225-232.

Enns LC, Canny MJ, McCully ME. 2000. An investigation of the role of solutes in the xylem sap and in the xylem parenchyma as the source of root pressure. Protoplasma **211**, 183–197.

Landsberg JJ, Fowkes ND. 1978. Water Movement Through Plant Roots. Annals of Botany **42**, 493-508.

Gambetta GA, Knipfer T, Fricke W, McElrone AJ. 2017. Aquaporins and Root Water Uptake. In: Chaumont F, Tyerman SD, eds. Plant Aquaporins: From Transport to Signaling: Springer International Publishing, 133–153.

Fiscus EL. 1975. The Interaction between Osmotic- and Pressure-Induced Water Flow in Plant Roots. Plant Physiology **55**, 917–922.

Fiscus EL. 1977. Determination of Hydraulic and Osmotic Properties of Soybean Root Systems. Plant Physiology **59**, 1013-1020.

Fiscus EL. 1986. Diurnal Changes in Volume and Solute Transport Coefficients of Phaseolus Roots. Plant Physiology **80**, 752-759.

Foster KJ, Miklavcic SJ. 2016. Modeling Root Zone Effects on Preferred Pathways for the Passive Transport of Ions and Water in Plant Roots. Frontiers in Plant Science **7**, doi: doi.org/10.3389/fpls.2016.00914.

Foster KJ, Miklavcic SJ. 2017. A Comprehensive Biophysical Model of Ion and Water Transport in Plant Roots. I. Clarifying the Roles of Endodermal Barriers in the Salt Stress Response. Frontiers in Plant Science **8**, doi: 10.3389/fpls.2017.01326.

Frensch J, Steudle E. 1989. Axial and Radial Hydraulic Resistance to Roots of Maize (Zea mays L.). Plant Physiology **91**, 719–726.

Accepted Manuscript

Downloaded from https://academic.oup.com/jxb/advance-article/doi/10.1093/jxb/erac471/6896019 by guest on 02 January 2023

Godin C, Caraglio Y. 1998. A Multiscale Model of Plant Topological Structures. Journal of Theoretical Biology **191**, 1-46.
Gonzalez-Tello P, Camacho F, Blazquez G. 1994. Density and Viscosity of Concentrated Aqueous Solutions of Polyethylene Glycol. Journal of Chemical & Engineering Data **39**, 611-614.
Gorska A, Zwieniecka A, Holbrook NM, Zwieniecki MA. 2008. Nitrate induction of root hydraulic conductivity in maize is not correlated with aquaporin expression. Planta **228**, 989-998.
Hachez C, Veselov D, Ye Q, Reinhardt H, Knipfer T, Chaumont WF, François. 2012. Short-term control of maize cell and root water permeability through plasma membrane aquaporin isoforms. Plant, Cell & Environment **35**, 185–198.
Heymans A, Couvreur V, Lobet G. 2021. Combining cross-section images and modeling tools to create high-resolution root system hydraulic atlases in Zea mays. Plant Direct **5**, doi: 10.1002/pld3.334.
Jackson MB, Davies W, Else MA. 1996. Pressure -Flow Relationships, Xylem Solutes and Root Hydraulic Conductance in Flooded Tomato Plants. Annals of Botany **77**, 17–24.
Knipfer T, Danjou M, Vionne C, Fricke W. 2021. Salt stress reduces root water uptake in barley (Hordeum vulgare L.) through modification of the transcellular transport path. Plant, Cell & Environment **44**, 458-475.
Knipfer T, Fricke W. 2010. Root pressure and a solute reflection coefficient close to unity exclude a purely apoplastic pathway of radial water transport in barley (Hordeum vulgare). New Phytologist **187**, 159–170.
Lobet G, Pagès L, Draye X. 2011. A Novel Image-Analysis Toolbox Enabling Quantitative Analysis of Root System Architecture. Plant Physiology **157**, 29–39.
Markhart AH, Smit B. 1990. Measurement of Root Hydraulic Conductance. HortScience **25**, 282–287.
Maurel C, Boursiac Y, Luu D-T, Santoni V, Shahzad Z, Verdoucq L. 2015. Aquaporins in Plants. Physiological Reviews **95**, 1321–1358.
Meunier F, Draye X, Vanderborght J, Javaux M, Couvreur V. 2017. A hybrid analytical-numerical method for solving water flow equations in root hydraulic architectures. Applied Mathematical Modelling **52**, 648–663.
Meunier F, Zarebanadkouki M, Ahmed MA, Carminati A, Couvreur V, Javaux M. 2018. Hydraulic conductivity of soil-grown lupine and maize unbranched roots and maize root-shoot junctions. Journal of Plant Physiology **227**, 31-44.
Michel BE. 1983. Evaluation of the Water Potentials of Solutions of Polyethylene Glycol 8000 Both in the Absence and Presence of Other Solutes. Plant Physiology **72**, 66-70.
Miller DM. 1985a. Studies of Root Function in Zea mays: III. Xylem Sap Composition at Maximum Root Pressure Provides Evidence of Active Transport into the Xylem and a Measurement of the Reflection Coefficient of the Root. Plant Physiology **77**, 162-167.
Miller DM. 1985b. Studies of Root Function in Zea mays: IV. Effects of Applied Pressure on the Hydraulic Conductivity and Volume Flow through the Excised Root. Plant Physiology **77**, 168–174.
Millet EJ, Welcker C, Kruijer W, et al. 2016. Genome-Wide Analysis of Yield in Europe: Allelic Effects Vary with Drought and Heat Scenarios Plant Physiology **172**, 749-764.
Murphy R. 2000. Some Compartmental Models of the Root: Steady-state Behavior. Journal of Theoretical Biology **207**, 557-576.
Passioura JB. 1988. Water Transport in and to Roots. Annual Review of Plant Physiology and Plant Molecular Biology **39**, 245–265.
Pradal C, Dufour-Kowalski S, Boudon F, Fournier C, Godin C. 2008. OpenAlea: a visual programming and component-based software platform for plant modelling. Functional Plant Biology **35**, 751-760.
Ramachandran P, Augstein F, Nguyen V, Carlsbecker A. 2020. Coping With Water Limitation: Hormones That Modify Plant Root Xylem Development. Frontiers in Plant Science **11**, doi: 10.3389/fpls.2020.00570.
Rosales MA, Maurel C, Nacry P. 2019. Abscisic Acid Coordinates Dose-Dependent Developmental and Hydraulic Responses of Roots to Water Deficit. Plant Physiology **180**, 2198-2211.

Accepted Manuscript

Downloaded from https://academic.oup.com/jxb/advance-article/doi/10.1093/jxb/erac471/6896019 by guest on 02 January 2023

Rüdinger M, Hallgren SW, Steudle E, Schulze E-D. 1994. Hydraulic and osmotic properties of spruce roots. Journal of Experimental Botany **45**, 1413-1425.
Steudle E. 1994. Water transport across roots. Plant and Soil **167**, 79–90.
Steudle E. 2000a. Water uptake by plant roots: an integration of views. Plant and Soil **226**, 45-56.
Steudle E. 2000b. Water uptake by roots: effects of water deficit. Journal of Experimental Botany **51**, 1531–1542.
Steudle E, Brinckmann E. 1989. The Osmometer Model of the Root: Water and Solute Relations of Roots of Phaseolus coccineus. Botanica Acta **102**, 85-95.
Virtanen P, Gommers R, Oliphant TE, et al. 2020. SciPy 1.0: fundamental algorithms for scientific computing in Python. Nature Methods **17**, 261-272.
Zarebanadkouki M, Meunier F, Couvreur V, Cesar J, Javaux M, Carminati A. 2016. Estimation of the hydraulic conductivities of lupine roots by inverse modelling of high-resolution measurements of root water uptake. Annals of Botany **118**, 853–864.

Accepted Manuscript

Downloaded from https://academic.oup.com/jxb/advance-article/doi/10.1093/jxb/erac471/6896019 by guest on 02 January 2023

Figure legends

Figure 1: Modeling water and solute transport within realistic RSAs of maize primary roots. (A) RSA of a CTR root with a heat map representation of the solute concentration. Scale bar: 10 mm. (B) The architecture was discretized in representative elementary volumes (REV). (C) Sketch of the different fluxes in and out of a REV, for $\boldsymbol{P_e > P_i > P_{i-1}}$ and $\boldsymbol{C_i > C_e}$ and in the absence of PEG. The sap flow along the xylem vessels is characterized by the axial conductance *K* profile. The water flow across the peripheral root tissues and into the xylem is characterized by the radial hydraulic conductivity *k*. The solutes are taken up into the xylem vessels at a constant rate J_s^*. P_s is the tissue permeability of the solutes. (D) REV geometry characterized by its length *l* and its diameter *d* that depends on the root order (axial or first order lateral root).

Figure 2: Representative examples of $J_v(P)$ curves in individual primary roots. (A, B) CTR roots. (C, D) PEG roots. (E, F) PEG-CTR roots. Dots represent experimental data, whereas solid curves indicate the best fit obtained with the model.

Figure 3: Flow of xylem sap exuded from excised roots at atmospheric pressure. CTR (black): n=8; PEG (green): n=8; PEG-CTR (orange): n=5. Each box indicates the 25th and 75th percentiles, while the line inside indicates the median value, and the T bars mark the 5th and 95th percentiles.

Figure 4: Representative examples of cut-and-flow data in individual primary roots. The data are derived from the same roots as in Figure 2. (A, B) CTR roots. (C, D) PEG roots. (E, F) PEG-CTR roots. Dots represent experimental data, whereas solid lines indicate the best fit obtained with the model.

Figure 5: Heat maps of driving components and radial water flux throughout the RSA of a CTR root (A, B and C), and a PEG root (D, E and F) bathing in a CTR or PEG solution, respectively. In both cases, a hydrostatic overpressure of 0.1 MPa was applied to the external medium. $\boldsymbol{\Delta P = P_e - P}$ is the difference between the hydrostatic pressure of the external medium, P_e, and the xylem vessel pressure *P*, in MPa (A and D). $\boldsymbol{\Delta C = C - C_e}$ is the difference between solute concentration in the xylem vessels, *C*, and the external concentration, C_e, in mol.m^{-3} (B and E). *j* is the local radial flow of water in µL.s^{-1}.m^{-2} (D and F). Scale bar: 10 mm.

Figure 6: Heat maps of driving components and radial flux throughout the RSA of a CTR root in a CTR solution and in conditions of spontaneous exudation (the bathing solution was at equilibrium with atmospheric pressure). Same notations and conventions as in Figure 5. Scale bar: 10 mm.

Figure 7: Variations of axial conductance (*K)* as a function of distance to root tip. The solid lines represent lowess fits done on *K* profiles of CTR roots (black; n = 8), PEG roots (green; n = 8), and PEG-CTR roots (orange; n=5). The dashed lines delineate the corresponding 95% confidence intervals.

Figure 8: Values of radial hydraulic conductivity (A), active solute uptake rate (B) and solute permeability (C) determined by inverse modeling in the indicated root types. Each box indicates the 25th and 75th percentiles, while the line inside indicates the median value, and the T bars mark the 5th and 95th percentiles. Corresponding individual values are shown with the same color on the left of each box plot.

Accepted Manuscript

Downloaded from https://academic.oup.com/jxb/advance-article/doi/10.1093/jxb/erac471/6896019 by guest on 02 January 2023

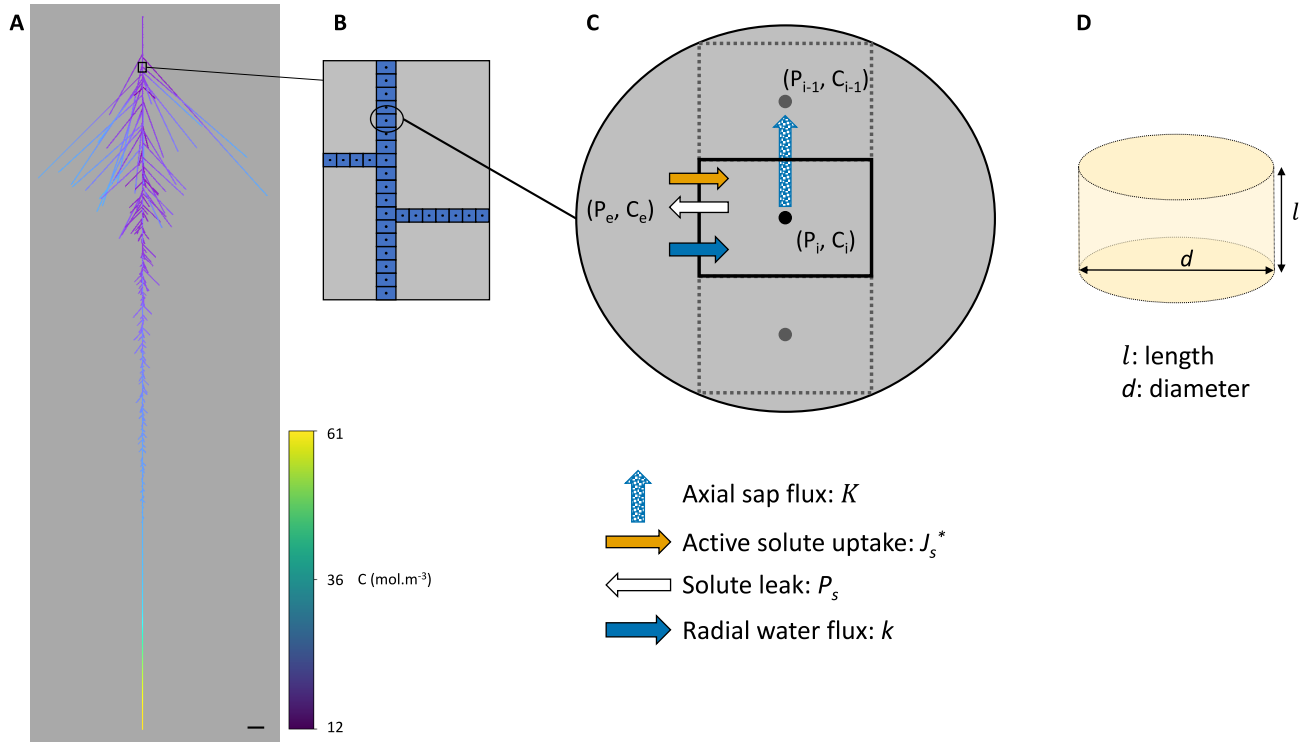

Figure 1: Modeling water and solute transport within realistic RSAs of maize primary roots. (A) RSA of a CTR root with a heat map representation of the solute concentration. Scale bar: 10 mm. (B) The architecture was discretized in representative elementary volumes (REV). (C) Sketch of the different fluxes in and out of a REV, for $P_e > P_i > P_{i-1}$ and $C_i > C_e$ and in the absence of PEG. The sap flow along the xylem vessels is characterized by the axial conductance K profile. The water flow across the peripheral root tissues and into the xylem is characterized by the radial hydraulic conductivity k. The solutes are taken up into the xylem vessels at a constant rate J_s^*. P_S is the tissue permeability of the solutes. (D) REV geometry characterized by its length l and its diameter d that depends on the root order (axial or first order lateral root).

Downloaded from https://academic.oup.com/jxb/advance-article/doi/10.1093/jxb/erac471/6896019 by guest on 02 January 2023

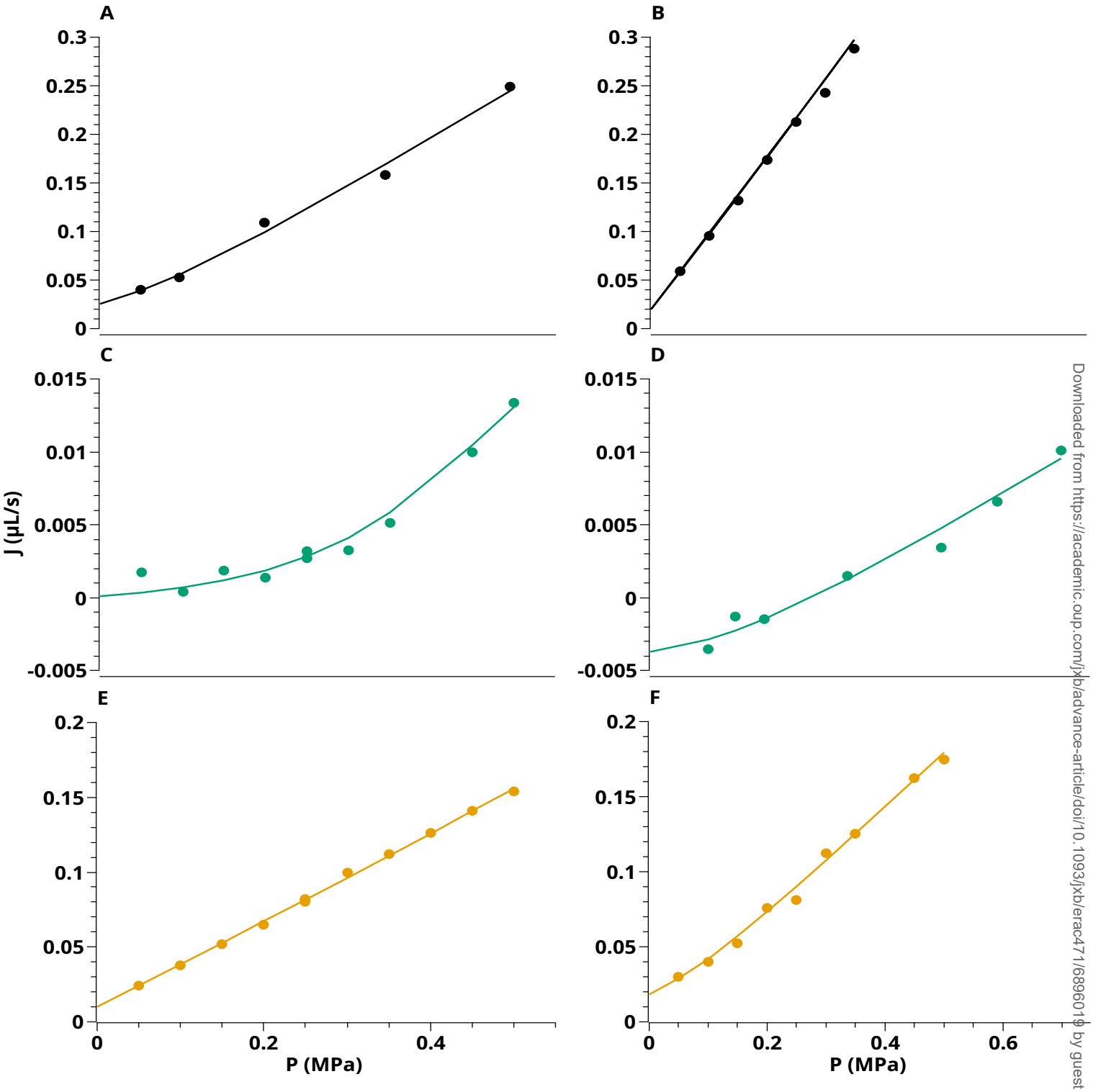

Downloaded from https://academic.oup.com/jxb/advance-article/doi/10.1093/jxb/erac471/6896019 by guest on 02 January 2023

Figure 2: Representative examples of $J_v(P)$ curves in individual primary roots. (A, B) CTR roots. (C, D) PEG roots. (E, F) PEG-CTR roots. Dots represent experimental data, whereas solid curves indicate the best fit obtained with the model.

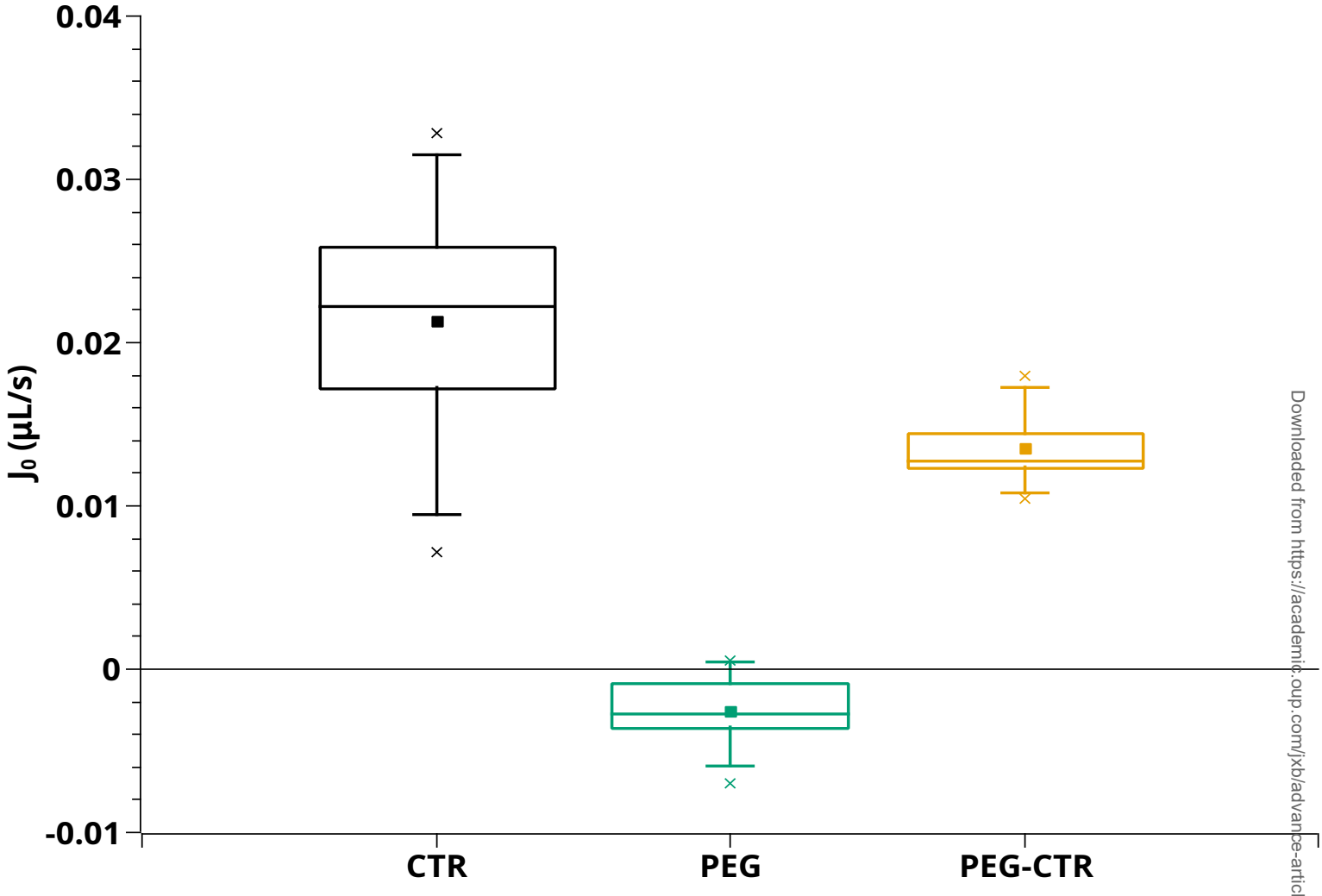

Figure 3: Flow of xylem sap exuded from excised roots at atmospheric pressure. CTR (black): n=8; PEG (green): n=8; PEG-CTR (orange): n=5. Each box indicates the 25th and 75th percentiles, while the line inside indicates the median value, and the T bars mark the 5th and 95th percentiles.

Downloaded from https://academic.oup.com/jxb/advance-article/doi/10.1093/jxb/erac471/6896019 by guest on 02 January 2023

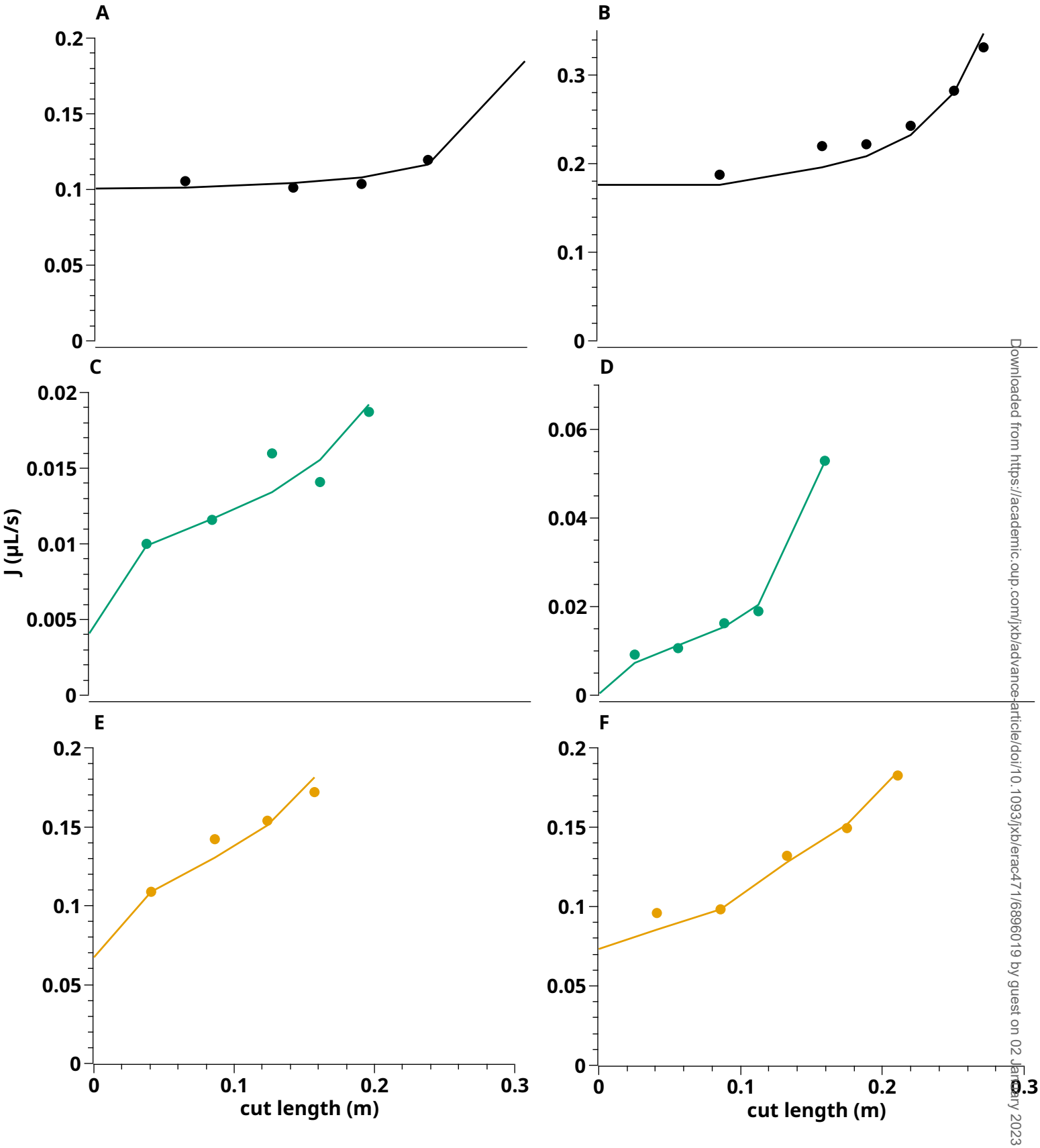

Downloaded from https://academic.oup.com/jxb/advance-article/doi/10.1093/jxb/erac471/6896019 by guest on 02 January 2023

Figure 4: Representative examples of cut-and-flow data in individual primary roots. The data are derived from the same roots as in Figure 2. (A, B) CTR roots. (C, D) PEG roots. (E, F) PEG-CTR roots. Dots represent experimental data, whereas solid lines indicate the best fit obtained with the model.

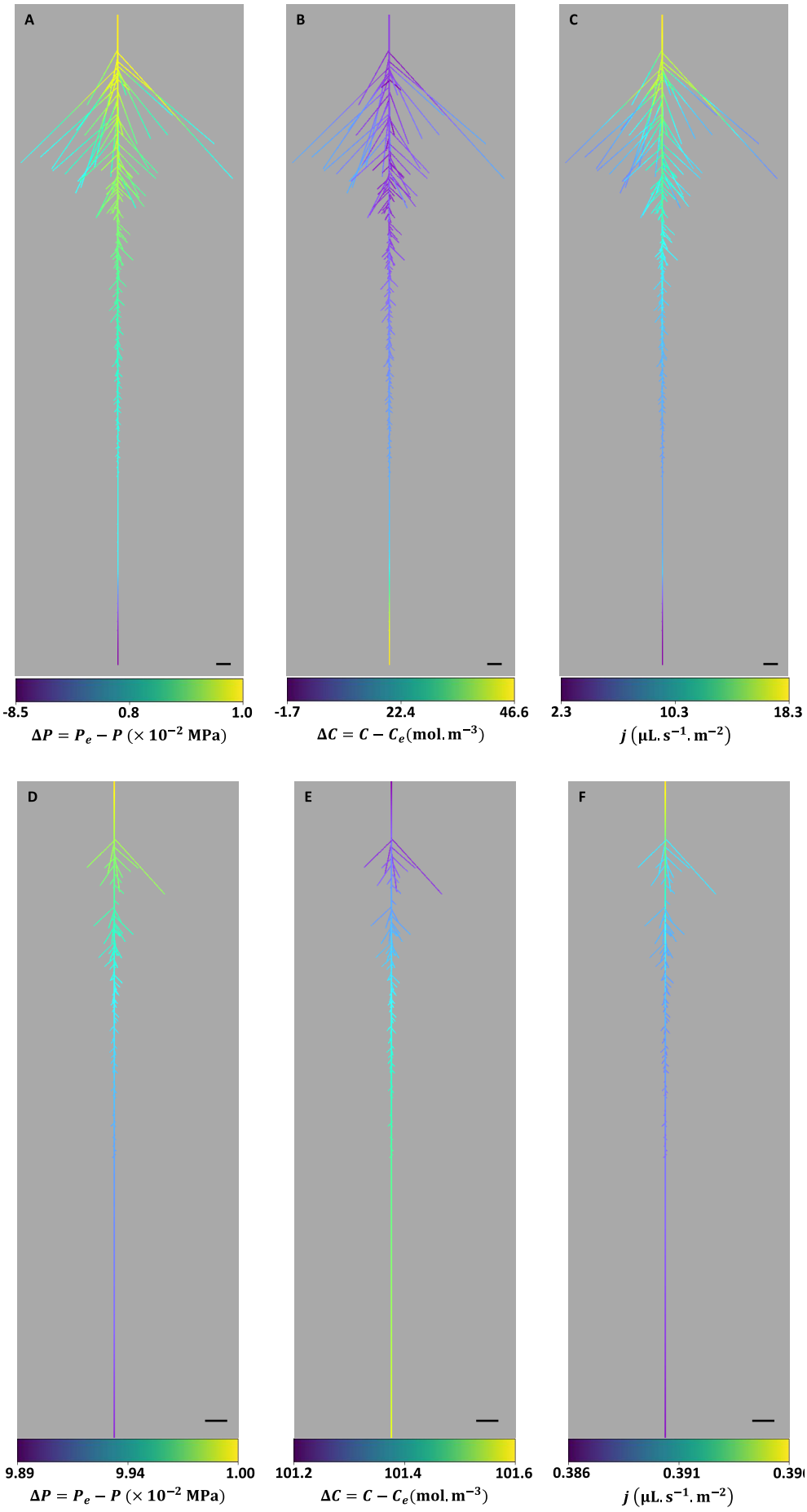

Figure 5: Heat maps of driving components and radial water flux throughout the RSA of a CTR root (A, B and C), and a PEG root (D, E and F) bathing in a CTR or PEG solution, respectively. In both cases, a hydrostatic overpressure of 0.1 MPa was applied to the external medium. $\Delta P=P_e-P$ is the difference between the hydrostatic pressure of the external medium, P_e, and the xylem vessel pressure P, in MPa (A and D). $\Delta C=C-C_e$ is the difference between solute concentration in the xylem vessels, C, and the external concentration, C_e, in mol.m^{-3} (B and E). j is the local radial flow of water in µL.s^{-1}.m^{-2} (D and F). Scale bar: 10 mm.

Downloaded from https://academic.oup.com/jxb/advance-article/doi/10.1093/jxb/erac471/6896019 by guest on 02 January 2023

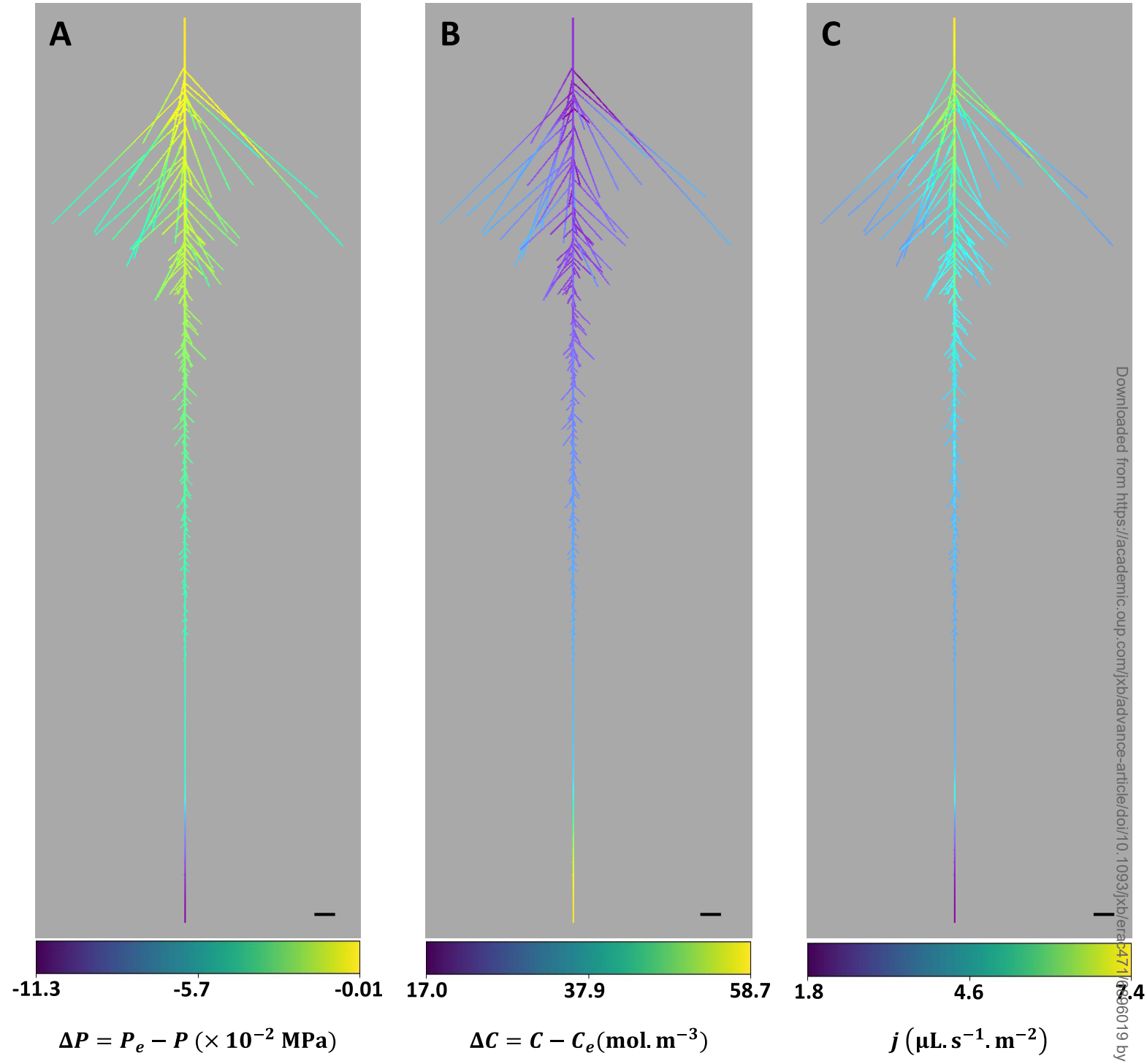

Figure 6: Heat maps of driving components and radial flux throughout the RSA of a CTR root in a CTR solution and in conditions of spontaneous exudation (the bathing solution was at equilibrium with atmospheric pressure). Same notations and conventions as in Figure 5. Scale bar: 10 mm.

Downloaded from https://academic.oup.com/jxb/advance-article/doi/10.1093/jxb/erad471/7336019 by guest on 02 January 2023

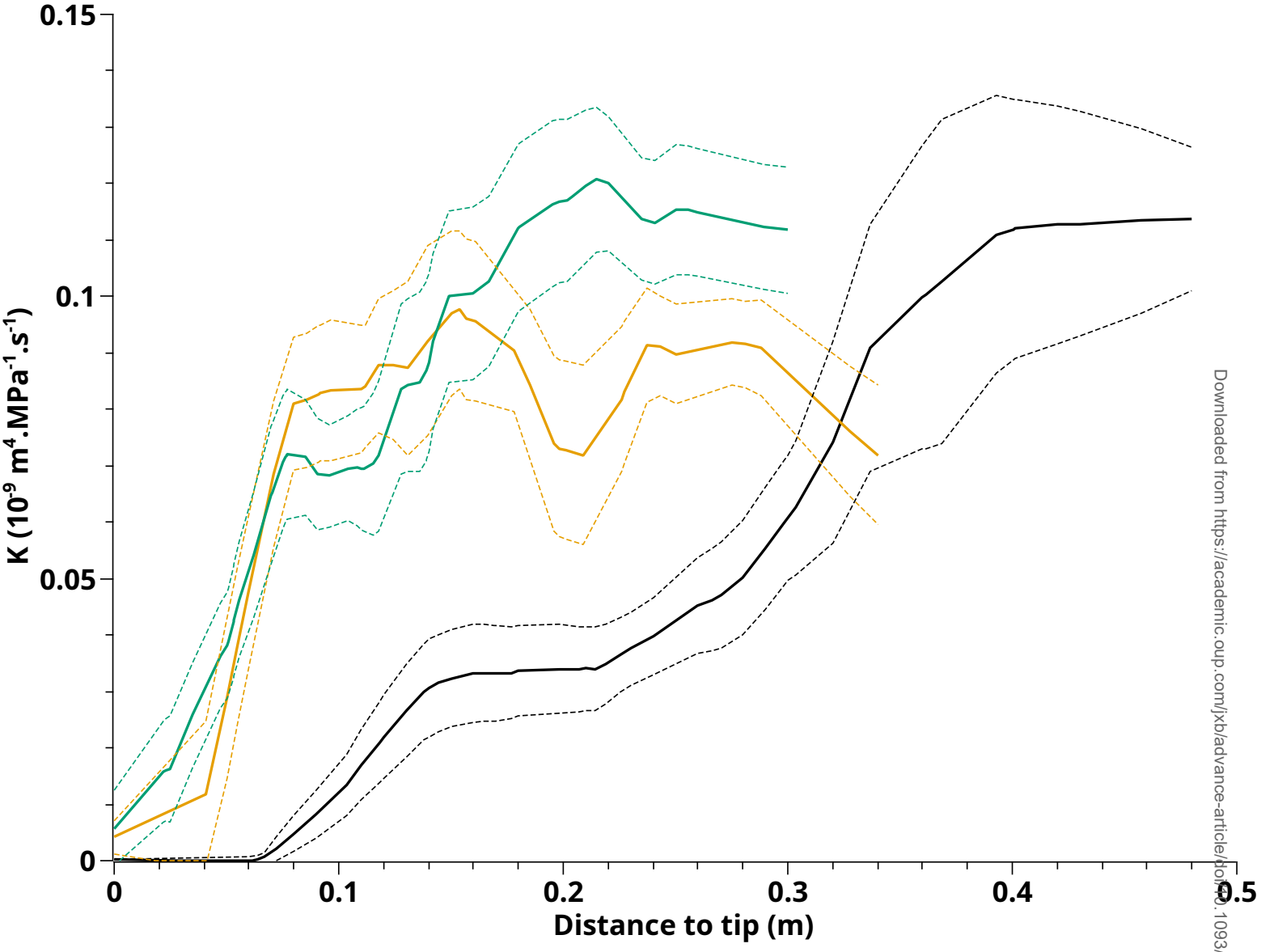

Figure 7: Variations of axial conductance (K) as a function of distance to root tip. The solid lines represent lowess fits done on K profiles of CTR roots (black; n = 8), PEG roots (green; n = 8), and PEG-CTR roots (orange; n=5). The dashed lines delineate the corresponding 95% confidence intervals.

Downloaded from https://academic.oup.com/jxb/advance-article/doi/10.1093/jxb/erac476/6896019 by guest on 02 January 2023

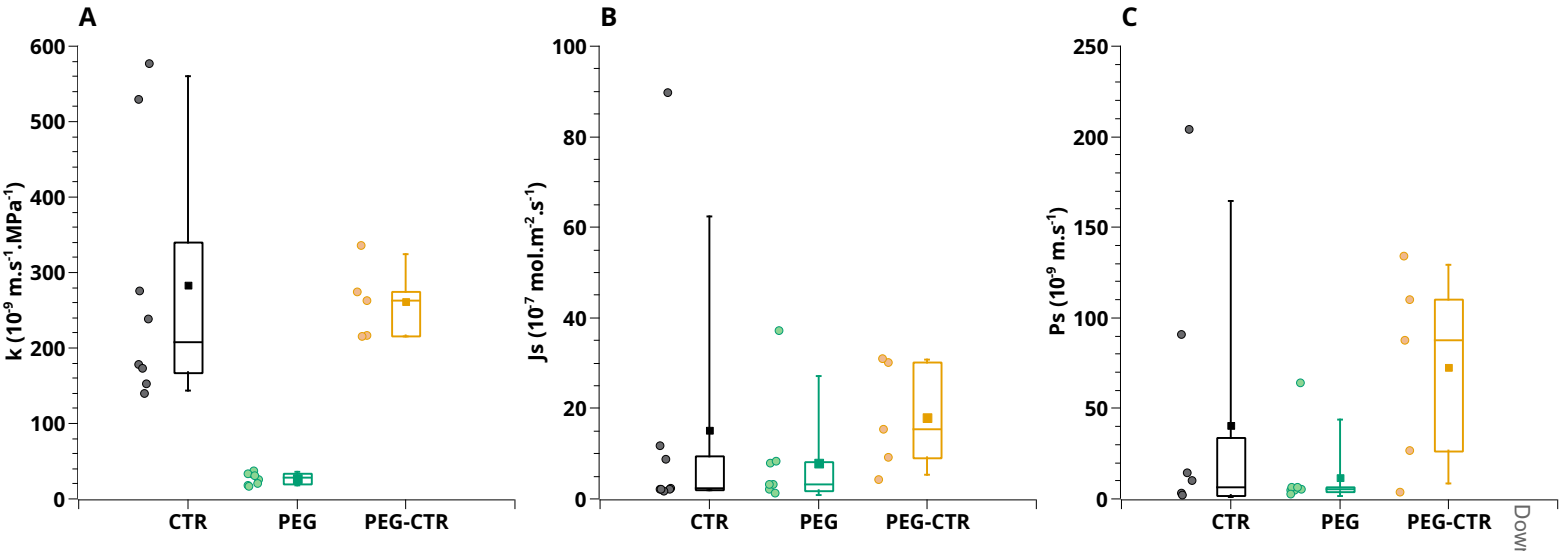

Figure 8: Values of radial hydraulic conductivity (A), active solute uptake rate (B) and solute permeability (C) determined by inverse modeling in the indicated root types. Each box indicates the 25th and 75th percentiles, while the line inside indicates the median value, and the T bars mark the 5th and 95th percentiles. Corresponding individual values are shown with the same color on the left of each box plot.

Downloaded from https://academic.oup.com/jxb/advance-article/doi/10.1093/jxb/erac471/6896019 by guest on 02 January 2023